Front. Chem. China 2010, 5(3): 331–341
DOI 10.1007/s11458-010-0004-0

RESEARCH ARTICLE

Real-time, single-particle measurements of ambient aerosols in Shanghai

Fan YANG, Xinning WANG, Yaping ZHANG, Xiaofei WANG, Hong CHEN, Xin YANG (✉) and Jianmin CHEN

As one of the major components of the earth's atmosphere, airborne particulate matter (or aerosol) has strong effects on air quality, regional and global climate, and human health. In ambient atmosphere, the different sources and complex evolutionary history of aerosol particles make the study of their chemical and physical properties extremely challenging. The invention of an online single-particle aerosol mass spectrometer provides a powerful technique to determine the size and chemical composition of individual aerosol particles in real time. We deployed an aerosol time-of-flight mass spectrometer (ATOFMS) to carry out single particle measurement in the urban area of Shanghai in the past few years. In this review paper, we summarize our recent work on the identification of particle type, mixing state and aging process, and the application of the individual particle information to the source apportionment of primary aerosol, and the investigation of the formation mechanism of secondary aerosol in Shanghai. The special capabilities of single particle mass spectrometry are proven essential to these studies. Multi-functional technique combinations of ATOFMS with other state-of-art aerosol instruments are also discussed for future studies.

Keywords aerosol, ATOFMS, particle classification, source apportionment, formation mechanism

1 Introduction

Aerosols or atmospheric particulates represent one of the major components of the earth's atmosphere. Aerosols can absorb and scatter radiation or act as cloud nuclei to significantly impact regional and global climate [1–4]. Aerosols can alter the chemical composition of the atmosphere through heterogeneous chemical reactions or other multiphase processes [5–8]. Aerosols can also spread toxic materials, biologic organisms, and pathogens, causing or enhancing respiratory, cardiovascular, infections, and diseases [9–11]. The effects of aerosols on air quality, climate, and human health are among the central topics in current environmental research. The size of ambient aerosols ranges from less than 10 nm to more than 10 μm in diameter. They originate from a wide variety of natural and anthropogenic sources with very complex compositions. These physical and chemical complexities can be enhanced even on a short time scale due to all kinds of aging processes and meteorological condition changes, which makes ambient aerosol measurement extremely challenging.

Tremendous efforts have been made in the development of instruments and techniques used for characterizing aerosols. Traditional methods normally include trapping aerosol particles through filtration or impaction followed by various sample extractions, and the results analyzed by GC, GC-MS, or LC-MS. However, these methods are not only time consuming but also suffer from the low sampling time resolution, sample loss (evaporation) or gain (adsorption), and unwanted chemical reactions during the extraction and analysis steps. Besides, filtration or impaction samples can only provide the averaged chemical composition and size distribution of an ensemble of particles, with no information about the differences among classes of particles such as dust, sea salt, soot, etc. An ideal aerosol analysis instrument would allow simultaneous determination of both physical and chemical characteristics in a single particle and obtained through real time sampling.

As an effort toward accomplishing these goals, a real time single-particle aerosol mass spectrometer was first developed by Murphy and Johnston in 1991 [12] and later by Prather and Nordmeyer [13]. This new technique can clearly distinguish different particle types. Moreover, each particle is analyzed within a second after entering the inlet of the machine, allowing detailed correlations to be drawn between single particle formation and meteorological conditions. Among different models, the aerosol time-of-flight mass spectrometer (ATOFMS) developed by Kimberly A. Prather and her team permits the complete analysis of both the size and chemical composition of individual aerosol particles in real time [13] and was commercialized by TSI. In the past two decades, real time single-particle aerosol mass spectrometry has been applied to many research areas including measurements in the free troposphere over the eastern Pacific Ocean and western coast of North America [14], the characterization of super fine particles and new particle formation [15], and the

Received January 15, 2010; accepted February 8, 2010
Department of Environmental Science & Engineering, Fudan University, Shanghai 200433, China
E-mail: yangxin@fudan.edu.cn

measurements of the density, optical property, reactivity and hygroscopicity of particles [16,17].

In China, rapid economic growth and urban development has heavily burdened the air quality especially in the east coast areas. Satellite observations have revealed severe aerosol pollution in eastern China with extremely high fine particle concentrations compared with the other areas in the world [18]. The aerosol pollution was primarily due to energy consumption and other human activities. Shanghai is the largest city and a major industrial center in eastern China, with a population of over 17 million. Industries in Shanghai range from petrochemical, textiles and metallurgy to paper production and food processing. Its air quality has been deteriorating in the past several decades. The annual average concentration of $PM_{2.5}$ (particles with an aerodynamic diameter of 2.5 μm or smaller) reached 94.6 $\mu g \cdot m^{-3}$ from 2003–2005 [19]. Numerous studies have been carried out on the characteristics of aerosol particles in Shanghai [20]. However, most of these studies were based on conventional filter sampling techniques for collecting the ambient aerosols with 12 – 24 h sampling time.

In the past few years, ATOFMS has been deployed in our group to measure the size and chemical composition of individual particles and their correlations with the fluctuation of gas phase pollutants and meteorological conditions in the urban area of Shanghai. The special capabilities of single particle mass spectrometry were proven essential to these studies [21–24]. In this review paper, we summarize our recent work, with a focus on the identification of particle type, mixing state of individual particles, source apportionment of primary aerosols, and formation mechanisms of the major secondary components of aerosols in the atmosphere of a highly polluted urban area.

2 Experimental

The ATOFMS (TSI model 3800) can analyze the size and composition of individual particles from a poly-disperse aerosol in real-time, providing information on the origin, reactivity, and fate of atmospheric aerosols. Figure 1 shows the schematic diagram of ATOFMS. The whole machine includes three major parts: (1) an aerosol introduction interface which includes an aerodynamic focus lens and three adjustable stages of differential pumping (2) a light scattering region for particle detection and velocity/size determination (3) a reflectron time-of-flight mass spectrometer for single particle composition analysis.

Aerosols are introduced into a vacuum region through the aerodynamic focus lens which is designed to effectively transmit particles in the size range of 100 nm to 3 μm. Each particle is accelerated to a size-dependent terminal velocity. Particles scatter light as they cross two orthogonal continuous diode-pumped green lasers, and the time taken for a particle to move between the two lasers is monitored by a logic circuit.

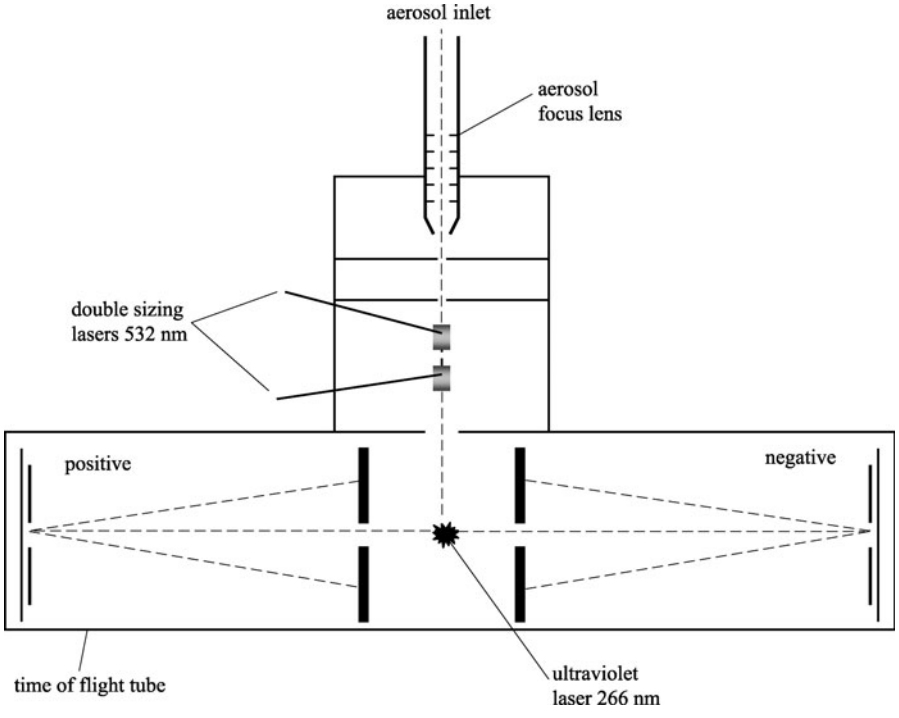

Figure 1 Schematic diagram of the ATOFMS configuration.

The particle size is measured from a calibration curve relating the velocity of the particle to an aerodynamic diameter. The firing of the desorption/ionization laser (Nd: YAG laser, 266 nm) is triggered based on the velocity measurement when the particle enters the center of the source region of the mass spectrometer. Both positive and negative ions generated from laser ablation are analyzed simultaneously by time-of flight mass spectrometry. The power density of the desorption/ionization laser was kept at about 1.0×10^8 W·cm^{-2} in our experiment. Polystyrene latex spheres (Nanosphere Size Standards, Duke Scientific Corp., Palo Alto) of 0.22 – 2.00 μm diameter were suspended using an atomizer (TSI-3076) to create monodispersed aerosols used for size calibration.

3 Aerosol sampling

The ATOFMS was located in the building of the Department of Environmental Science and Engineering, Fudan University. This site is near residential, traffic, and construction emissions sources and basically represents an urban area. Ambient aerosols were transferred to the ATOFMS through a copper pipe 4 m long with an outer diameter about half an inch. A cyclone was used on the inlet and pulled 101 min·L^{-1} in the main sampling line to minimize the particle residence time in the sampling line and interaction with the tube wall. The inlet of the sampling tube was about 5 m above the ground and 0.5 m above the roof of the building. Ambient measurements were made almost 24 h continuously each day during sampling times. In this paper, we focus on the experimental data taken in August 2007 and February, March and December in 2008.

The local meteorological data including temperature, relative humidity (RH), visibility, wind speed and direction were provided by the Shanghai Meteorological Bureau. The daily average concentrations of PM_{10}, SO_2 and NO_2 were obtained from the Air Pollution Index (API) reported by the Shanghai Environment Protection Bureau (http://www.envir.gov.cn/).

4 Particle classification

Because of the huge amount of data collected by ATOFMS, typically tens to hundreds of thousands of particles with both positive and negative mass spectra per day, we need to employ statistical or neural network chemo-metric treatments to classify particles into a relatively small number of groups for drawing messages from data easily [25,26]. In our group, we used both mass spectral markers for certain aerosol types and the adaptive resonance theory (ART) neural network to classify the mass spectra.

4.1 Classification by mass spectral markers

Special mass spectral markers obtained by laboratory or ambient experiments for certain particle types have been proven to be highly useful in identifying major sources of primary urban aerosol particles. For example, elemental signals of vanadium and nickel are often excellent makers of oil combustion aerosol [27]. In our research [22, 23], we use the mass spectral markers based on previous studies [28] and our laboratory studies to classify all the particles into four major aerosol types in the order of dust, sodium-containing, carbonaceous, and biomass burning aerosols. The rest are regarded as only containing secondary species such as sulfate, nitrate, or ammonium. ATOFMS markers for major particle types are shown in Table 1. The classification followed the rules: (1) whenever a particle contains ion signals of dust signatures, it is classified as dust, (2) of the remaining particles, any containing a signal of sodium are classified as sodium, (3) of the remaining particles, any containing a signal of carbon are classified as carbon, (4) of the particles in sodium and carbon classes, any containing a signal of biomass burning are classified as biomass burning, and (5) the remaining particles are classified as pure secondary.

Figure 2 shows the distinct mass spectral patterns of the particles from five major aerosol types. For dust particles, peaks for Li^+ (m/z 7), Na^+ (m/z 23), Mg^+ (m/z 24), Al^+ (m/z 27), Ca^+ (m/z 40) and CaO^+ or Fe^+ (m/z 56) are present in the positive ion spectra. In the negative ion spectra, chloride (m/z −35 and −37), silicates (m/z −60 and −76), and phosphate (m/z −63 and −79) ions were regularly detected. The common occurrence of a great amount of nitrate (m/z −46 and −62) and sulfate (m/z −32, −80, −96, and −97) demonstrates how transformed the dust particles are in the Shanghai atmosphere. The sodium-containing particle shown in Figure 2 is a typical fresh sea salt particle characterized by the intense ion signals of Na^+, K^+ (m/z 39), Na_2OH^+ (m/z 63), Na_2Cl^+ (m/z 81) in the positive spectrum and F^- (m/z 19), Cl^- and phosphate in the negative spectrum. The carbonaceous particle in Figure 2 can be viewed as a "pure" elemental carbon (EC) particle by showing dominant carbon cluster ion signals in both positive and negative spectra. Actually, other members of the carbon group such as organic carbon (OC) particles or OC/EC mixture can also be sorted out by different spectral markers. The biomass burning particles are identified by the presence of extremely strong signals of K^+, K_2Cl^+ (m/z 113, 115), $K_3SO_3^+$ (m/z 197), $K_3SO_4^+$ (m/z 213) in the positive spectra, and CN^- (m/z 26) and levoglucosan (m/z −45, −59,

Table 1 Summary of the ATOFMS markers used to search for the major particle types observed in Shanghai

species	$\Delta(m/z)$	marker ion	area	relative area	function
sodium	23±0.5	$[Na]^+$	100	0.04	
dust	25.5 – 28	$[Al]^+$	1500		or
	54 – 57	$[Fe]^+$	1500		or
	1.2 – 2.2	$[H]^+$	1500		or
	5 – 9	$[Li]^+$	200		or
	40±0.5	$[Ca]^+$	2500		or
	96±0.5 and no 72±0.5	$[CaO]^+$	100		
carbon	12±0.5	$[C]^+$	50	0.005	or
	36±0.5	$[C_3]^+$	50	0.005	or
	37±0.5	$[C_3H]^+$	50	0.005	or
	60±0.5	$[C_5]^+$	50	0.005	or
	72±0.5	$[C_6]^+$	50	0.005	or
	−(12±0.5)	$[C]^-$	50	0.005	or
	−(24±0.5)	$[C_2]^-$	50	0.005	or
	−(36±0.5)	$[C_3]^-$	50	0.005	or
	−(48±0.5)	$[C_4]^-$	50	0.005	or
	−(72±0.5)	$[C_6]^-$	50	0.005	
biomass burning	38.2 – 41.5	$[K]^+$	1500		and
	11 3±0.5, 115±0.5	$[K_2Cl]^+$	50	0.005	or
	197±0.5	$[K_3SO_3]^+$	50	0.005	or
	213±0.5	$[K_3SO_4]^+$	50	0.05	or
	−(45±0.5)	$[CHO_2]^-$	50	0.05	or
	−(59±0.5)	$[C_2H_3O_2]^-$	50	0.05	or
	−(73±0.5)	$[C_3H_3O_2]^-$	50	0.05	or
nitrate	−46	$[NO_2]^-$	1000		or
	−(62±0.5)	$[NO_3]^-$	1000		
sulfate	−(97.5 – 95.5)	$[HSO_4]^-/[C_6]^+$	100		
ammonium	18±0.5	$[NH_4]^+$	30		

− 73) in the negative spectra. Particles in the secondary class usually show intense signals of sulfate and nitrate in the negative mass spectra while the positive spectra are characterized by hydrocarbon envelopes with high mass positive ions up to 300 Da.

4.2 Classification by ART-2a

Compared with the manual classification by mass spectral markers as discussed above, the ART neural network provides an objective standard for the sorting of mass spectrometry. The ART neural network is an efficient method of intelligently finding clusters in data sets with large numbers of variables. ART has the ability to add a new class if a data point falls outside of a preset proximity to all existing classes. In this way, it can identify new categories of data as they emerge without disturbing the existing categories. The most recent incarnation of the method is a particularly efficient execution called the ART-2a algorithm [29]. Particles with sufficiently similar mass spectral patterns were grouped into one class by ART-2a automatically when classified.

The parameters for the ART-2a analysis in our study include a vigilance factor of 0.5, a learning rate of 0.05, a maximum of 20 iterations, and a range of the first 250 mass-to-charge (m/z) units of mass spectra. Using this method, we carried out a series of classifications for the metal (Pb, Zn, and Cu) containing particles in the atmosphere in Shanghai. For example, fine Zn-containing particles detected in winter 2008 were classified into five major groups based on the chemical compositions: nitrate, OC-sulfate, Mn-Pb, EC, and dust. For the submicron Cu-containing particles observed in summer 2007, seven distinct groups were identified which were labeled as vanadium, sulfate, chlorine, nitrate, EC, calcium, and iron [24]. As discussed in the next part of this paper, the identification of these sub-groups of particles and the fluctuation of their number concentrations (with wind direction) make the source apportionment of these particles possible.

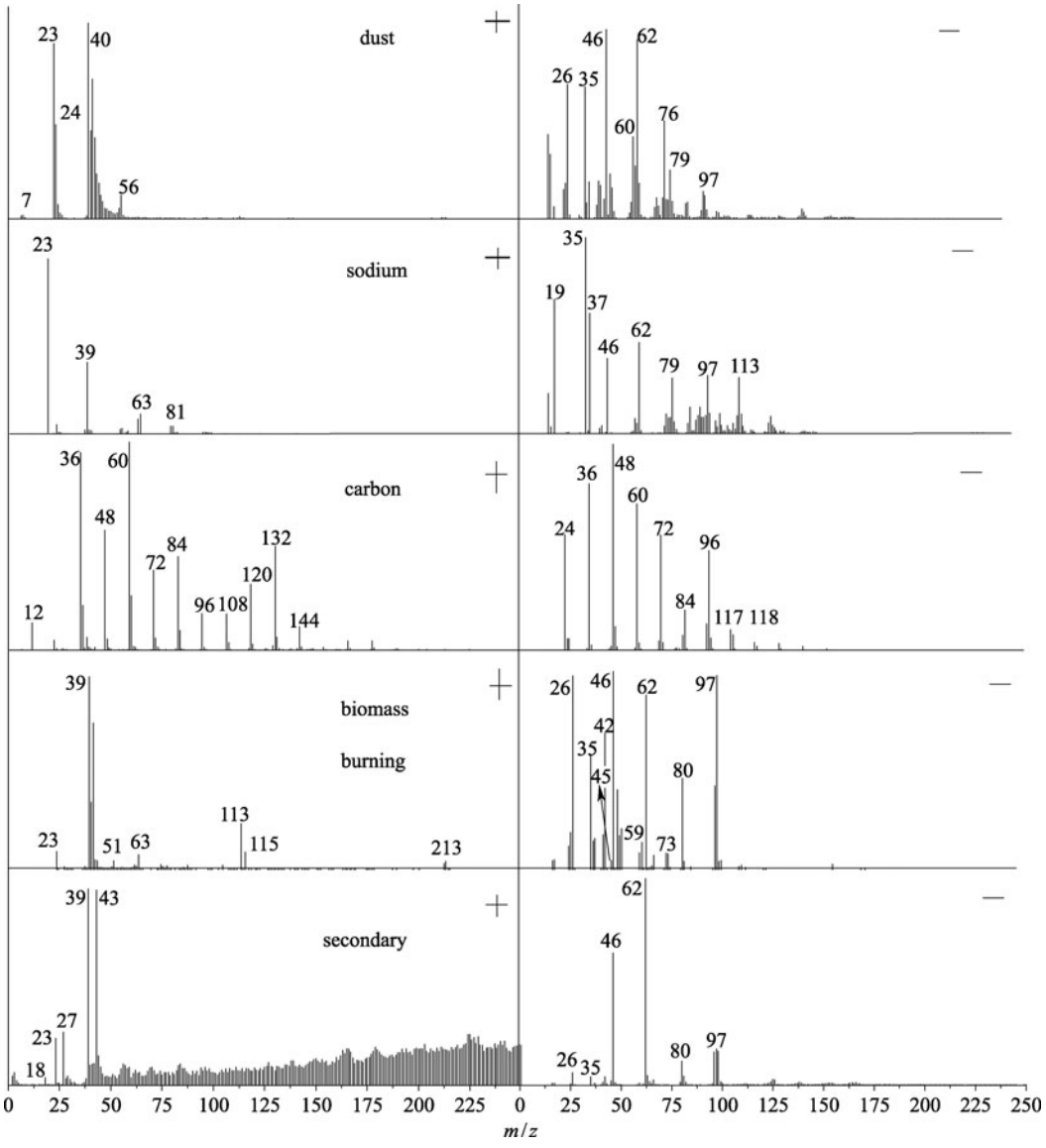

Figure 2 Typical mass spectra of a single particle from five major aerosol types.

5 Source apportionment of primary aerosol

In situ source apportionment is a major bright spot for the application of ATOFMS in atmospheric aerosol studies. Harrison's team used an ATOFMS to study aerosols in Athens during the summer of 2003 and found that dust from nearby roads or long range transport accounts for up to 49.5% of the particles characterized in Athens [30]. Ambient measurements with ATOFMS in the northern part of Mexico City by Prather's team showed that major sources of biomass burning particles in Mexico City were wood smoke from regional fires, cooking, incineration, agricultural fires, and refuse burning [31].

We had analyzed the sources of lead-containing particles in Shanghai in summer 2007 [21]. Emission sources were identified by analyzing individual particle data including particle size, chemical compositions, temporal variations of different chemical species and their close correlations. Based on the ART-2a classification, fine Pb-rich particles were subdivided into eight main classes by their mass spectral patterns, including: 1) OC-sulfate, 2) phosphate, 3) nitrate, 4) EC, 5) chlorine, 6) potassium rich, 7) sea salt, and 8) iron. Among these groups, OC-Sulfate and EC, which make up 45% of the total Pb-rich particles, can be viewed as two subgroups of carbonaceous particles. The correlated temporal profiles of the ATOFMS counts of these two classes ($R = 0.74$) indicates that they might come from the same emission sources. Both classes have strong sulfate signals compared with other classes, indicating that uptake of sulfuric acid takes place efficiently on these carbonaceous particles. Combustion

processes, such as vehicle exhaust and coal combustion are major sources of carbonaceous particles. In Shanghai, coal combustion facilities are the most important contributors to atmospheric lead-containing particles [19] rather than vehicle exhaust [32]. Thus, we assign the above carbonaceous particles to direct emission from coal combustion facilities. This assignment is further confirmed by the same size distribution (unscaled ATOFMS data) of these two classes.

Meanwhile, Pb-rich particles showed enrichment in chlorine. Lead can react with chloride during combustion, and waste incineration is a chlorine-rich combustion process. Sources of chloride in the waste streams include organic chlorides and inorganic chlorides (table salts such as sodium chloride) from kitchen waste. A widely used plastic, polyvinyl chloride (PVC) accounts for 80% of organically bounded Cl and 50%–65% of total Cl in municipal waste [33]. Pb^+ and Cl^- are well correlated in nitrate ($R = 0.77$), chlorine ($R = 0.86$) and potassium rich ($R = 0.73$) classes, suggesting that particles in these three classes might come from waste incineration. The highest number of concentrations of phosphate-rich particles occurred on August 4 and 5, 2007. During these two days, air parcels were mostly from the south or slightly south-east of the sampling site passing through the southern suburban districts of Shanghai (as shown in Figure 3(a)). Along the wind's trajectory, there are two large phosphate fertilizer factories. The stability of lead phosphate may

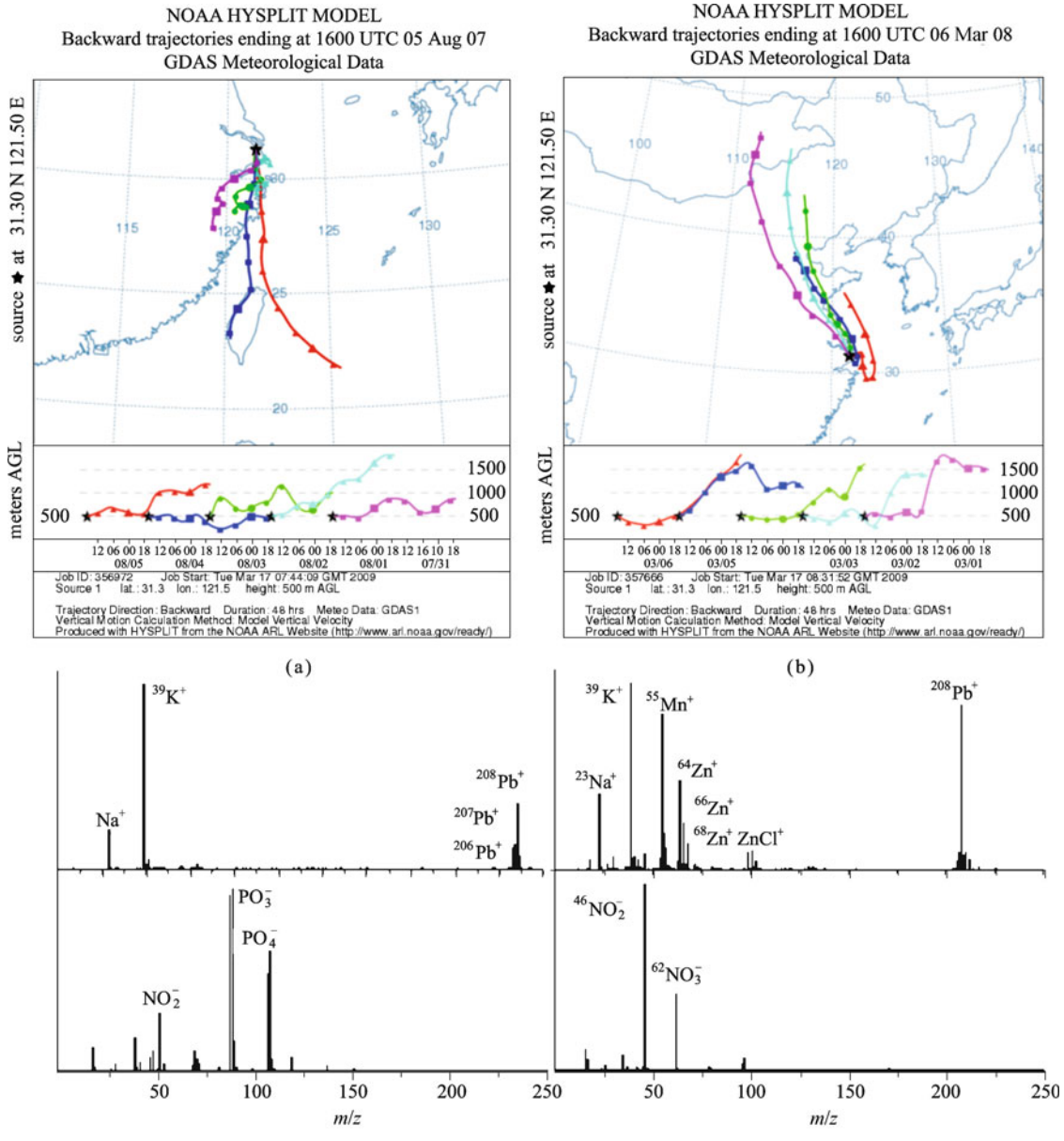

Figure 3 Comparisons of the air parcels backward trajectories and the corresponding mass spectra of Pb-containing particles in different seasons in Shanghai.

explain the frequent appearance of phosphate signals in this experiment. Phosphate fertilizers used in agriculture might introduce strong phosphate signals to this Pb-containing class at the same time.

Unlike the pollution patterns in summer, air pollution during the winter season in Shanghai is usually the worst time in a year due to poor atmospheric dispersion and the prevailing wind direction from heavily polluted areas (north and west) as shown in Figure 3(b). During February and March in 2008, we did a comparative analysis for the source apportionment of lead, zinc, copper and manganese containing particles [24]. Different with the observation in summer 2007, we found a large number of zinc, copper and manganese containing particles in winter and their number concentrations correlated well with Pb-containing particles ($R_{\text{Zn-Pb}} = 0.76$, $R_{\text{Mn-Pb}} = 0.60$, $R_{\text{Zn-Mn}} = 0.61$). Moreover, there are many Pb-containing particles also containing Zn and (or) Cu, suggesting that all these metal elements might come from the same source. Murphy's group had made the same observation in the United States in 2007. Through wind analysis, they found that most of the Pb/Zn containing particles came from the iron and steel plant [34]. As the biggest metallurgic company in Yangtze River delta, Bao Steel is located 13 km north from the sampling point. According to the temporal variation of the number concentration and wind direction analysis, these heavy metal containing particles were attributed to coal combustion and metal smelting emissions. Long distance transport from the northern areas of China also contributed a lot to the heavy metal containing particles in Shanghai during winter.

Figure 3 shows the comparisons of the backward trajectories of air parcels and the corresponding mass spectra of Pb-containing particles in different seasons in Shanghai. On August 7, 2007, wind from the south carried fresh Pb-containing particles with strong phosphate signals, which was attributed to local phosphate fertilizer industry emission (Figure 3(a)). On March 6, 2008, strong wind from the northwest brought in aged (strong nitrate signals) Pb-containing particles with coexistence of Mn and Zn, suggesting the long distance transport of metallurgic industry emissions.

6 Formation mechanism of secondary aerosol

Besides the primary aerosols which are directly emitted from natural or anthropogenic sources, tremendous amounts of particulate materials come from the secondary formation processes such as nucleation of gas phase molecules and multiple-phase reactions. Secondary aerosols (components) can significantly change the chemical and physical properties of primary aerosols, hence influencing the behavior of the regional atmosphere and even global climate change. High atmospheric pollution levels in the urban areas of China create favorable conditions for the formation of secondary aerosols. By taking advantage of ATOFMS, we carried out the investigation of the formation mechanisms of nitric acid and secondary oxalic acid in Shanghai.

6.1 Formation mechanism of particulate nitrate in Shanghai

Nitrate is one of the major inorganic components of urban aerosol particles. It is mainly formed from gas-to-particle partitioning in the atmosphere and is usually identified as a typical secondary aerosol component. Nitrate containing particles had been examined by our group in August 2007 [22] As shown in Figure 4(a), the relative intensity of nitrate signals showed a pronounced diurnal profile, peaking late at night or in early morning during highly polluted days (August1-5, 2007), which was closely correlated with the ambient relative humidity (RH). Similar observations have been reported in previous field studies (mostly in the United States) [35–37] and attributed to the gas-to-particle partitioning of NH_4NO_3 precursors (gaseous HNO_3 and NH_3), which is favored by lower temperature and higher RH. However, the negative correlation ($R = -0.6$) between the signals of ammonium and nitrate in the mass spectra (as shown in Figure 4(a)) excluded the possibility of NH_4NO_3 as a major form of particulate nitrate in our experiment. The relative intensity of nitrate tightly matched the RH variation, revealing a nitrate formation process driven by the water content in aerosol.

The peak intensities of nitrate during the nighttime and high concentrations of O_3 and NO_2 strongly suggest that the heterogeneous reactions of N_2O_5 and NO_3 on the aerosol surface dominated the particulate nitrate formation during our measurement. During the nighttime, nitrate radical NO_3 formed by the oxidation of NO_2 (by O_3) can react with NO_2 to form N_2O_5 which is the only source of N_2O_5 in the atmosphere. Because NO_3 is only present at significant concentrations at night due to its rapid photolysis this is restricted to the dark. N_2O_5 hardly reacts with water vapor, but it is easily hydrolyzed on a wet particle surface. NO_3 radicals can also be hydrolyzed on wet surfaces. Hydrolysis of NO_3 and N_2O_5 are the major formation channels of particulate nitrate during the nighttime.

However, the formation pathway of particulate nitrate was quite different in winter in Shanghai. During the experiment in December 2008, much more ammonium containing particles were observed with stronger relative intensities compared with those in summer. As shown in Figure 4(b), the relative intensity of ammonium signals correlated well ($R = 0.75$) with that of nitrate, suggesting that ammonium nitrate is the major form of particulate nitrate in winter.

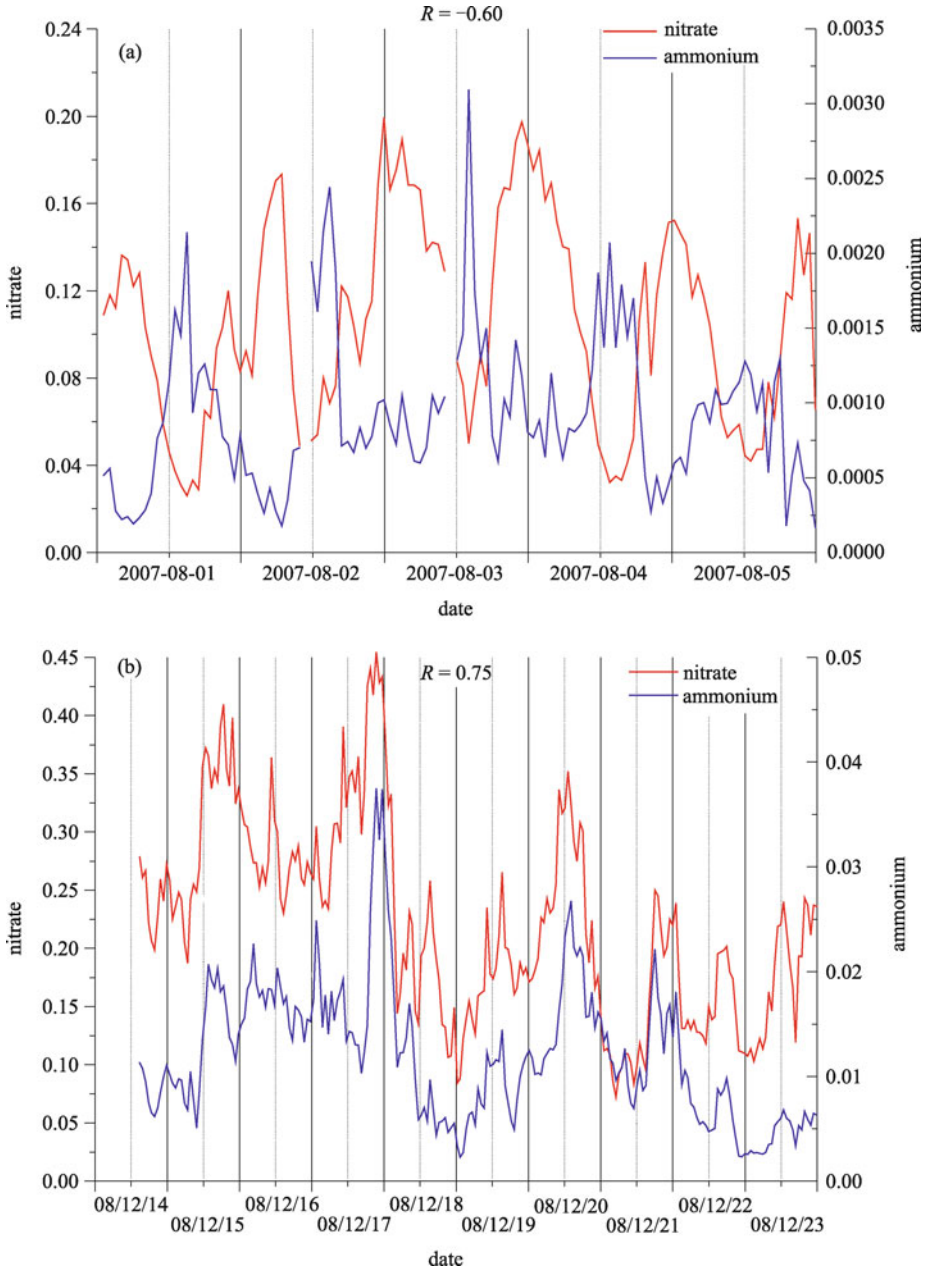

Figure 4 Correlation between the concentrations of particulate nitrate and ammonium in (a) summer and (b) winter.

6.2 Formation mechanisms of secondary oxalic acid in Shanghai

Oxalic acid, as one of the abundant and important low molecular weight dicarboxylic acids in the atmosphere, has received increasing attention in recent years because of its potential to alter the hygroscopic properties of aerosols and its roles in influencing submicron particles to act as Cloud Condensation Nuclei (CCN) [38]. Oxalic acid in individual aerosol particles was measured using ATOFMS in the summer of 2007.

Different from the purely secondary species such as sulfuric acid and nitric acid, oxalic acid can be produced directly from biomass burning, coal combustion and vehicular emissions [39]. During our experiment, the high ratio (21%) of biomass burning particles in the oxalate-containing particles and their relatively simple chemical histories (only 13.5% can be viewed as aged) reveal the contributions of biomass burning as a major primary source of oxalic acid in Shanghai. Biomass burning events in China are commonly in the form of crop residue burning in summer and autumn, mostly occurring during the daytime. The average diurnal variation of the biomass burning class confirms this point by showing higher particle counts from 8:00 am to 6:00 pm.

For the secondary oxalic acid in aerosol, evidences for two different formation pathways were observed [23]. First, the number fraction of oxalate-containing particles in the total collected particles was not stable during the sampling period, but it correlated well with that of sulfate particles. Meanwhile, 82.6% of the oxalate-containing particles were internally mixed with sulfate, much higher than the sulfate-containing ratio (47.6%) in the total particles. Air parcel backward trajectories showed that, during the sampling time with high ratio of oxalate-containing particles, air-masses passed through 1500 m above ground level, indicating possible penetrations of the cloud boundary layer. These observations suggest that in-cloud processing played an important role in the formation of oxalic acid during our sampling period.

Moreover, oxalate and sulfate particles shared a similar particle size distribution as shown in Figure 5(a), which is strong evidence for in-cloud formation. However, the particle size with the highest number concentration located at about 0.45 μm in Figure 5(a), is too small compared with the reported values for in-cloud processing (~0.7 μm [40,41]). We note that the size distribution here is based on particle counts rather than mass concentration, which is usually the case in the previous size segregation measurements. If we assume that the density and the mole concentration of sulfate or oxalate are the same for all the particles, the size distributions based on mass concentration will be reshaped as in Figure 5(b), which clearly shows a bimodal distribution for both oxalate and sulfate. The droplet

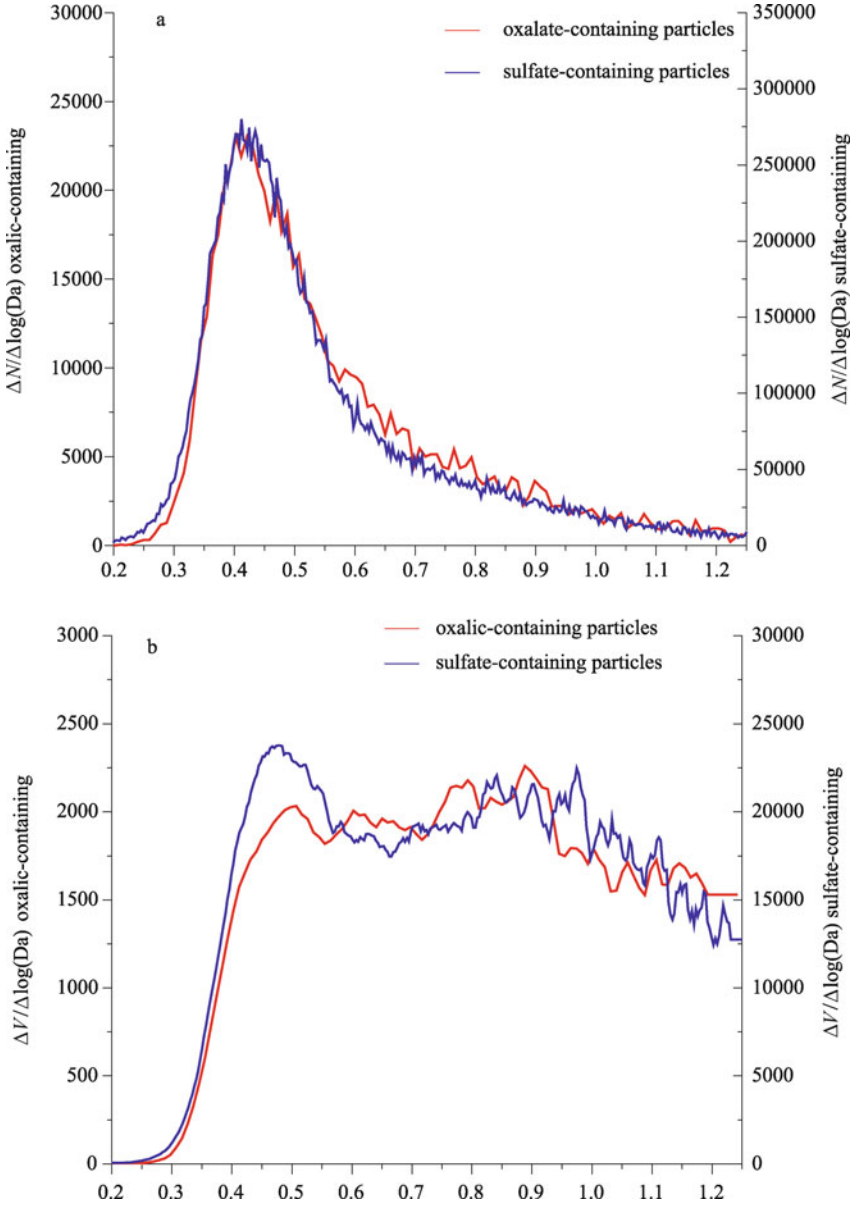

Figure 5 Size distributions of Oxalate-containing particles and Sulfate-containing particles based on (a) particle counts and (b) volume (mass).

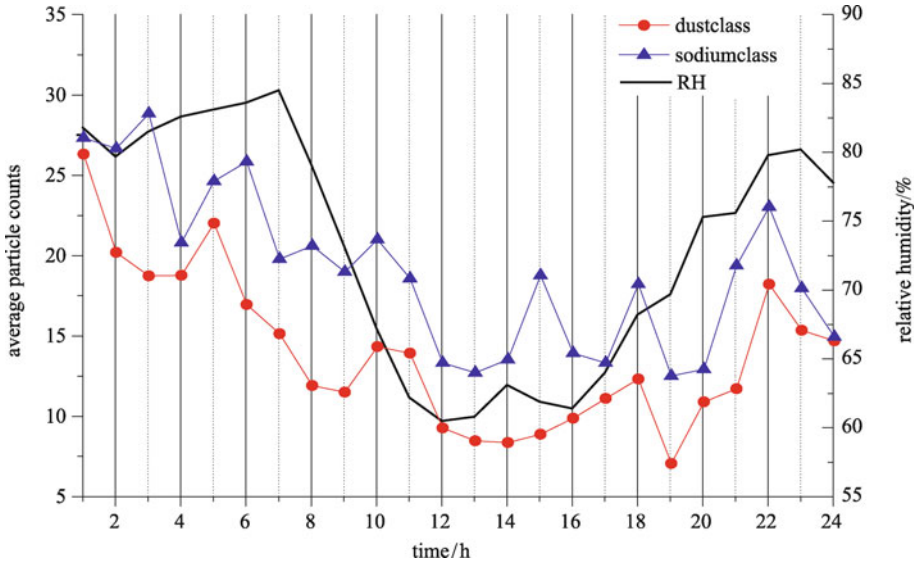

Figure 6 Average diurnal variation of the oxalate-containing particle counts for Dust, Sodium classes. The ambient RH variation during the sampling period is also shown.

mode in 0.8–0.9 μm can be attributed to in-cloud processes [40,41].

In-cloud formation of oxalic acid mainly depends on the frequency and duration of clouds and would not show the dependence on the original particle composition or produce extended diurnal cycles. However, the diurnal patterns of dust and sodium-containing (mostly sea salt) particles fitted well with the RH variation (as shown in Figure 6), suggesting that non-cloud aqueous oxidation or heterogeneous reactions occurring in hydrated/deliquesced aerosols during elevated humidity at night might also contribute to the oxalic acid production. In our experiment, the ratios of dust and sodium-containing classes in the oxalate-containing particles were higher than those in the total particles. The enrichment of oxalic acid in mineral dust and sea salt particles is a further evidence of the coexistence of non-cloud mechanisms since the chemistry of the original particles plays more important roles in hydrated/deliquesced aerosols [42]. The alkaline dust particles in Asia have a high affinity for acids including gas-phase oxalic acid from photo-oxidation, and sea salt particles with high hygroscopicity would take up more water content during elevated humidity.

7 Summary

The ATOFMS system, which is designed for online analysis of individual aerosol particles, provides a powerful approach to determine aerosol composition and size distribution simultaneously in real time. Messages from the measurements made by this instrument have been widely used qualitatively to study both the sources of ambient aerosols and the transformation of particles in atmosphere. Taking advantage of ATOFMS we carried out a series of investigations in the urban areas of Shanghai, focusing on the identification of the type, mixing state and evolutionary history of individual particles. The particle-resolved physical and chemical information has been used for the detailed analysis of the sources of heavy metal containing particles, as well as the formation mechanism of typical secondary aerosols in Shanghai.

ATOFMS can also work together with other state-of-the-art instruments as an online mass detector to form a powerful, multi-functional technique combination. We are planning to combine ATOFMS with other aerosol instruments such as the scan mobility particle sizer (SMPS), hygroscopic tandem differential mobility analyzer (HTDMA), and laser cavity ring-down spectrometer (LCRS) to further explore the hygroscopicity, light scattering and absorbing properties of aerosols together with their chemical information. We believe that ATOFMS, including other online aerosol mass spectrometers, will play an increasingly important role in the near future in the atmospheric research field in China.

Acknowledgements The authors thank the State Key Development Program for Basic Research of China (Grant No. 2008CB417205) from The Ministry of Science and Technology of China and the National Natural Science Foundation of China (Grant Nos. 20937001, 40875074) for the support.

References

1. Seinfeld, J. H.; Pandis, S. N., *Atmospheric Chemistry & Physics*; John Wiley & Sons: New York, 1998
2. Ramanathan, V.; Chung, C.; Kim, D.; Bettge, T.; Buja, L.; Kiehl,

J. T.; Washington, W. M.; Fu, Q.; et al., *Proc. Natl. Acad. Sci. U. S.A*. **2005**, *5*, 1053–1123
3. Ramanathan, V.; Crutzen, P. J.; Kiehl, J. T.; Rosenfeld, D., *Science* **2001**, *294*, 2119–2124
4. Lohmann, U., *J. Atmos. Chem. Phys* **2005**, *5*, 715–737
5. Ravishankara, A. R., *Science* **1997**, *276*, 1058–1065
6. Abbatt, J. P., *Chem. Rev*. **2003**, *103*, 4783–4800
7. Finlayson-Pitts, B. J., *Chem. Rev*. **2003**, *103*, 4801–4822
8. Maria, S. F.; Russell, L. M.; Gilles, M. K.; Myneni, S. C. B., *Science* **2004**, *306*, 1921–1924
9. Bernstein, J. A.; Alexis, N.; Barnes, C.; Bernstein, I. L.; Bernstein, J. A.; Nel, A.; Peden, D.; Diaz-Sanchez, D.; et al., *J. Allergy Clin. Immunol*. **2004**, *114*, 1116–1123
10. Finlayson-Pitts, B. J.; Pitts, J. N. Jr, *Science* **1997**, *276*, 1045–1051
11. Hinds, W. C., *Aerosol Technology*, Wiley: New York, 1999
12. McKeown, P. J.; Johnston, M. V.; Murphy, D. M., *Anal. Chem*. **1991**, *63*, 2069–2073
13. Prather, K. A.; Nordmeyer, T.; Salt, K., *Anal. Chem*. **1994**, *66*, 1403–1407
14. Murphy, D. M.; Cziczo, D. J.; Hudson, P. K.; Schein, M. E.; Thomson, D. S., *Aerosol Science* **2004**, *35*, 135–139
15. Johnston, M. V., *J. Mass Spectrom*. **2000**, *35*, 585–595
16. Buzorius, G.; Zelenyuk, A.; Brechtel, F.; Imre, D., *Geophys. Res. Lett*. **2002**, *29*, 1974
17. Moffet, R. C.; Prather, K. A., *Anal. Chem*. **2005**, *77*, 6535–6541
18. Tie, X.; Brasseur, G.; Zhao, C.; Granier, C.; Massie, S.; Qin, Y.; Wang, P. C.; Wang, G. L.; et al., *Atmos. Environ*. **2006**, *40*, 2607–2625
19. Wang, Y.; Zhuang, G.; Zhang, X.; Huang, K.; Xu, C.; Tang, A.; Chen, J.; An, Z., *Atmos. Environ*. **2006**, *40*, 2935–2952
20. Chan, C. K.; Yao, X., *Atmos. Environ*. **2008**, *42*, 1–42
21. Zhang, Y.; Wang, X.; Chen, H.; Yang, X.; Chen, J.; Allen, J. O., *Chemosphere* **2009**, *74*, 501–507
22. Wang, X.; Zhang, Y.; Chen, H.; Yang, X.; Chen, J.; Geng, F., *Environ. Sci. Technol*. **2009**, *43*, 3061–3066
23. Yang, F.; Chen, H.; Wang, X.; Yang, X.; Du, J.; Chen, J., *Atmos. Environ*. **2009**, *43*, 3876–3882
24. Zhang, Y.; Yang, F.; Wang, M.; Wang, X.; Chen, H.; Yang, X., *J. Fudan Univer. (Nat. Sci.)* **2009**, (in press)
25. Fergenson, D. P.; Song, X. H.; Ramadan, Z.; Allen, J. O.; Hughes, L. S.; Cass, G. R.; Hopke, P. K.; Prather, K. A., *Anal. Chem*. **2001**, *73*, 3535–3541
26. Phares, D. J.; Rhoads, K. P.; Wexler, A. S.; Kane, D. B.; Johnston, M. V., *Anal. Chem*. **2001**, *73*, 2338–2344
27. Campen, M. J.; Nolan, J. P.; Schladweiler, M. C. J.; Kodavanti, U. P.; Evansky, P. A.; Costa, D. L.; Watkinson, W. P., *Toxicol. Sci*. **2001**, *64*, 243–252
28. Liu, D. Y.; Wenzel, R. J.; Prather, K. A., *J. Geophys. Res*. **2003**, *108*, 8426
29. Song, X. H.; Hopke, P. K.; Fergenson, D. P.; Prather, K. A., *Anal. Chem*. **1999**, *71*, 860–865
30. Dall'Osto, M.; Harrison, R. M., *Atmos. Environ*. **2006**, *40*, 7614–7631
31. Moffet, R. C.; de Foy, B.; Molina, L. T.; Molina, M. J.; Prather, K. A., *Atmos. Chem. Phys*. **2008**, *8*, 4499–4516
32. Chen, J.; Tan, M.; Li, Y.; Zhang, Y.; Lu, W.; Tong, Y.; Zhang, G.; Li, Y., *Atmos. Environ*. **2005**, *39*, 1245–1253
33. Keane, M. A., *J. Chem. Technol. Biot*. **2007**, *82*, 787–795
34. Murphy, D. M.; Hudson, P. K.; Cziczo, D. J.; Gallavardin, S.; Froyd, K. D.; Johnston, M. V.; Middlebrook, A. M., *Atmos. Chem. Phys*. **2007**, *7*, 3195–3210
35. Lee, S. H.; Murphy, D. M.; Thomson, D. S.; Middlebrook, A. M., *J. Geophys. Res*. **2003**, *108*, 8417–8424
36. Zheng, J.; Zhang, R.; Fortner, E. C.; Volkamer, R. M.; Molina, L.; Aiken, A. C.; Jimenez, J. L.; Gaeggeler, K.; et al., *Atmos. Chem. Phys*. **2008**, *8*, 6823–6838
37. Zhang, Q.; Canagaratna, M. R.; Jayne, J. T.; Worsnop, D. R.; Jimenez, J. L., *J. Geophys. Res*. **2005**, *110*, doi:10.1029/2004JD004649
38. Facchini, M. C.; Mircea, M.; Fuzzi, S.; Charlson, R. J., *Nature* **1999**, *401*, 257–259
39. Yamasoe, M. A.; Artaxo, P.; Miguel, A. H.; Allen, A., *Atmos. Environ*. **2000**, *34*, 1641–1653
40. Yao, X.; Fang, M.; Chan, C. K., *Atmos. Environ*. **2002**, *36*, 2099–2107
41. Yao, X.; Lau, A. P. S.; Fang, M.; Chan, C. K.; Hu, M., *Atmos. Environ*. **2003**, *37*, 3001–3007
42. Sullivan, R. C.; Prather, K. A., *Environ. Sci. Technol*. **2007**, *41*, 8062–8069